EPJ Web of Conferences **93**, 02005 (2015)
DOI: 10.1051/epjconf/20159302005

Measurement of reaction cross-sections for ^{89}Y at average neutron energies of 7.24-24.83 MeV

Muhammad Zaman[1], Guinyun Kim[1,a], Haladhara Naik[1, 2], Kwangsoo Kim[1], Muhammad Shahid[1]

[1]*Department of Physics, Kyungpook National University, Daegu 702-701, Republic of Korea*
[2]*Radiochemistry Division, Bhabha Atomic Research Centre, Trombay, Mumbai- 40085, India*

Abstract. We measured neutron-induced reaction cross-sections for ^{89}Y(n,γ)^{90m}Y and ^{89}Y(n,α)^{86}Rb reactions with the average neutron energy region from 7.45 to 24.83 MeV by an activation and off-line γ-ray spectrometric technique using the MC-50 Cyclotron at Korea Institute of Radiological and Medical Sciences. The neutron-induced reaction cross-sections of ^{89}Y as a function of neutron energy were taken from the TENDL-2013 library. The flux-weighted average cross-sections for ^{89}Y(n,γ)^{90m}Y and ^{89}Y(n,α)^{86}Rb reactions were calculated from the TENDL-2013 values based on mono-energetic neutron and by using the neutron energy spectrum from MCNPX 2.6.0 code. The present results are compared with the flux-weighted values of TENDL-2013 and are found to be in good agreement

1 Introduction

Photon and neutron induced reaction cross-sections of various materials in a wide range of energies are important for different applications such as the design of radiation shielding, the calculation of absorbed dose in the human body during radiotherapy, the activation analysis, and the physics and technology of fusion and fission reactors [1]. Yttrium is naturally mono-isotopic and nontoxic material and has good physical properties [2]. Neutron, photon, and proton-induced reaction cross-sections of yttrium are important for its application in making X-ray intensifying screen and laser. Yttrium is also used as alloys with other materials as the control rod for power reactors [3].

The interest in high-energy neutrons is rapidly growing because of a number of potential applications in nuclear science and technology concerning fast neutrons. In the high-energy region above ~20 MeV, a truly mono-energetic neutron beam is not feasible in a strict sense. For certain nuclear reactions, there is a strong dominance of neutrons in a narrow energy range and are called quasi-mono energetic neutron sources [4]. Quasi-mono energetic neutrons based on the ^{7}Li(p,n)^{7}Be reaction with flexibility in energy and shape of neutron field is controllable in the energy range 11-175 MeV [5-8].

The ^{89}Y(n,γ)^{90m}Y and ^{89}Y(n,α)^{86}Rb reaction cross-sections were reported with various mono-energetic neutron beam in the energy range from threshold to 15.8 MeV [9]. There is no experimental data exist for higher neutron energies. In the present work, we have determined the neutron-induced reaction cross-sections of yttrium in the average neutron energies of 7.45 to 24.83 MeV from ^{9}Be(p,n) reaction and by an activation and off-line γ-spectrometry technique using proton beam from the MC-50 Cyclotron at the Korea Institute of Radiological and Medical Sciences (KIRAMS). The theoretical reaction cross-section values based on mono-energetic neutron beam were taken from the TENDL-2013 library [10]. The neutron spectrum for ^{9}Be(p,n) reaction was calculated with the MCNPX 2.6.0 code [11].

2 Experimental set-up

The experiment was carried out by using the MC-50 cyclotron at KIRAMS. In the present work proton beam of energy 25, 35, and 45 MeV were impinging on 5 mm Be target producing neutrons from the ^{9}Be(p,n) reaction. The experimental details and sample characteristics are given in our previous work [12].

The neutron energy spectra for three different proton energies were estimated by using the MCNPX 2.6.0 code [12]. The flux-weighted neutron energies for the ^{89}Y(n,γ)^{90m}Y and ^{89}Y(n,α)^{86}Rb reactions from their threshold energy (E_{th}) to the maximum neutron energy (E_{max}) based on the neutron spectrum in Fig. 1 were estimated for three proton energies as follows:

$$\langle E_n \rangle = \int_{E_{th}}^{E_{max}} E_n \phi(E_n) dE_n \Big/ \int_{E_{th}}^{E_{max}} \phi(E_n) dE_n \qquad (1)$$

where $\phi(E_n)$ is the neutron flux as a function of neutron energy, E_n. The flux-weighted neutron energies for ^{89}Y(n,γ)^{90m}Y and ^{89}Y(n,α)^{86}Rb reactions with a 45 MeV proton beams are 18.05 and 24.83 MeV, respectively. Those for a 35 MeV proton beam are 13.41 and 18.22 MeV for ^{89}Y(n,γ)^{90m}Y and ^{89}Y(n,α)^{86}Rb reactions. For a 25

[a] Corresponding author: gnkim@knu.ac.kr

MeV proton beam the flux-weighted neutron energy is 7.45 and 12.95 MeV.

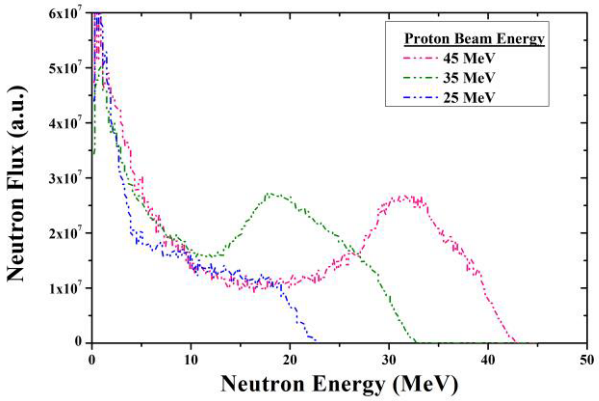

Figure 1. The calculated neutron spectra produced by the ^{9}Be(p,n) reaction using MCNPX code.

The irradiated ^{89}Y sample along with Al wrapper was taken out from the irradiated assembly after 30 minutes and mounted on Perspex plates. The γ-ray counting of the reaction products from the ^{89}Y sample and ^{27}Al wrapper was done by using an energy- and efficiency-calibrated HPGe detector coupled to a PC-based 4 K-channel analyzer. The γ-ray counting was done for at least three half-lives in live time mode. The high energy neutrons flux causes different reactions in ^{89}Y target.

3 Data analysis

The aluminium wrapper were used as neutron flux monitor. The photo-peak area of 1368.6 keV observed in the γ-ray spectrum was due to the formation of ^{24}Na from the ^{27}Al(n,α)^{24}Na reaction was used to determine the neutron flux. The net photo-peak areas of the different γ-rays of reaction products of interest were calculated by subtracting the Compton background from the gross peak area. The numbers of observed γ-rays (N_{obs}) under 1368.6 keV photo-peak are related to the cross section $\sigma_R(E_n)$ for the ^{27}Al(n,α)^{24}Na reaction and the integrated neutron flux $\Phi_n (= \int_{E_{th}}^{E_{max}} \phi(E_n) dE_n)$ as follows [13]:

$$N_{obs}\left(\frac{CL}{LT}\right) = \frac{n\sigma_R(E_n)\Phi_n I_\gamma \varepsilon\left(1-e^{-\lambda T_I}\right)e^{-\lambda T_C}\left(1-e^{-\lambda CL}\right)}{\lambda} \quad (2)$$

where n is the number of target atom, I_γ is the branching intensity of the analysed γ-ray, ε the detection efficiency, λ is the decay constant ($=ln2/T_{1/2}$) of the isotope of interest, T_I, T_C, CL and LT are the irradiation time, the cooling time, the real time, and the counting time, respectively. The integrated neutron flux Φ_n for each irradiation condition was obtained from the reaction threshold (3.245 MeV) of the ^{27}Al(n,α)^{24}Na reaction to the maximum neutron energies of 23, 33, and 43 MeV as shown in Fig. 1. However the threshold energies for the ^{89}Y(n,γ)^{90m}Y and ^{89}Y(n,α)^{86}Rb reactions are zero and 6.6 MeV, respectively. Thus the integrated neutron flux obtained from the ^{27}Al(n,α)^{24}Na reaction has to change based on threshold energies of the ^{89}Y(n,γ)^{90m}Y and ^{89}Y(n,α)^{86}Rb reactions. Then the integrated neutron flux ratios for the ^{89}Y(n,γ)^{90m}Y and ^{89}Y(n,α)^{86}Rb reactions were obtained from the threshold to the maximum neutron energy divided by the flux from the reaction threshold (3.245 MeV) of the ^{27}Al(n, α)^{24}Na reaction to the maximum neutron energies obtained by using the MCNPX 2.6.0 code as shown in Fig. 1. The detailed calculations of flux factors are given in our earlier work [12]. Using the factors, the integrated neutron fluxes for the individual reactions were obtained. Then the flux-weighted average cross-sections for ^{89}Y(n,γ)^{90m}Y and ^{89}Y(n,α)^{86}Rb reactions were calculated as follows:

$$\langle\sigma\rangle = \frac{N_{obs}(CL/LT)\lambda}{n\Phi_n I_\gamma \varepsilon\left(1-e^{-\lambda T_I}\right)e^{-\lambda T_C}\left(1-e^{-\lambda CL}\right)}. \quad (3)$$

The nuclear spectroscopic data used for determining the cross-sections values were taken from refs. [14,15].

4 Results and discussion

The flux-weighted average cross-sections of the ^{89}Y(n,γ)^{90m}Y and ^{89}Y(n,α)^{86}Rb reaction were determined in the present work and listed in Table 1. The uncertainties in the measured cross-sections are briefly discussed in our earlier work [12] and are in between 16 and 20% based on a statistical error of 10-13% and a systematic error of 12-15%.

The cross-sections of ^{89}Y(n,γ)^{90m}Y and ^{89}Y(n,α)^{86}Rb reaction with mono-energetic neutrons are available in the literature [9]. However, we could not compare directly the present flux-weighted average cross sections with the literature data measured with mono-energetic neutrons. The cross-sections of ^{89}Y as a function of neutron energy were taken from TENDL-2013 nuclear data library [10], based on TALYS-1.6 code. The flux-weighted average cross-sections were obtained by using the following equation:

$$\langle\sigma\rangle = \frac{\int_{E_{th}}^{E_{max}} \sigma(E_n)\phi(E_n)dE_n}{\int_{E_{th}}^{E_{max}} \phi(E_n)dE_n}, \quad (4)$$

where $\sigma(E_n)$ is the cross-section for the ^{89}Y(n,γ)^{90m}Y and ^{89}Y(n,α)^{86}Rb reaction with a mono-energetic neutron, taken from TENDL-2013. The neutron flux $\phi(E_n)$ is estimated by the MCNPX 2.6.0 code as shown in Fig. 1. The flux-weighted average cross-sections of ^{89}Y(n,γ)^{90m}Y and ^{89}Y(n,α)^{86}Rb reactions based on Eq. (4) are given in Table 1. It can be seen from Table 1 that the flux-weighted average cross-sections of ^{89}Y(n,γ)^{90m}Y and ^{89}Y(n,α)^{86}Rb reactions obtained from TENDL-2013 based on the TALYS 1.6 agree in general with the present experimental results.

The ^{89}Y(n,γ)^{90m}Y and ^{89}Y(n,α)^{86}Rb reaction cross-sections for mono-energy neutron from TENDL-2013 are plotted in Fig. 2 and Fig. 3. and compared with experimental data from literature [9]. Our experimental data and flux weighted average value of TENDL-2013 are also plotted in Figs. 2 and 3. Our experimental data are found to be in good agreement, which indicates the correctness of the present approach.

Table 1. The average cross-sections of $^{89}Y(n,\gamma)^{90m}Y$ and $^{89}Y(n,\alpha)^{86}Rb$ reactions.

Average neutron energy (MeV)	$^{89}Y(n, \gamma)^{90m}Y$ cross section (mb)		$^{89}Y(n,\alpha)^{86}Rb$ cross section (mb)	
	Experiment	TENDL-2013	Experiment	TENDL-2013
7.45	0.20 ±0.03	0.203		
12.95			---	5.358
13.41	1.00 ±0.20	0.158		
18.05	1.12 ±0.21	0.132		
18.22			5.22 ±1.04	9.303
24.83			7.10 ± 1.41	7.42

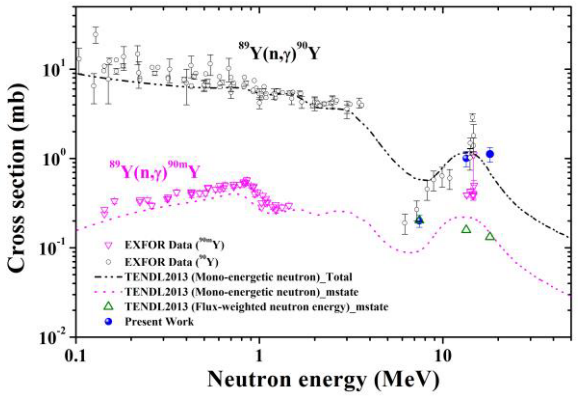

Figure 2. The $^{89}Y(n,\gamma)^{90m}Y$ reaction cross-sections from literature [9] and those obtained from the TENDL-2013 [10] as a function of mono-energetic neutron energy.

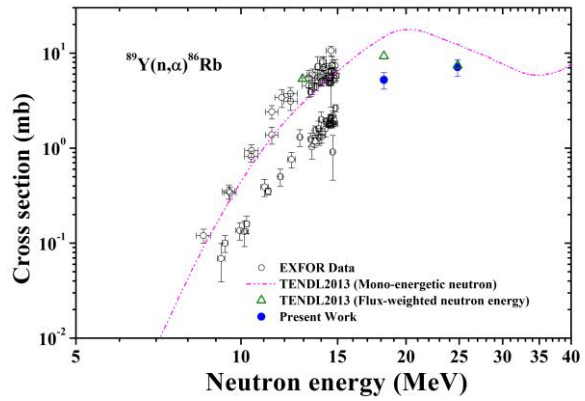

Figure 3. The $^{89}Y(n,\alpha)^{86}Rb$ reaction cross-sections from literature [9] and those obtained from the TENDL-2013 [10] as a function of mono-energetic neutron energy.

Acknowledgements

The authors would like to express their sincere thanks to the staff of the MC-50 Cyclotron in the KIRAMS for the excellent operation and their support during the experiment. This research was partly supported by the Institutional Activity Program of KAERI Institute, by the National Research Foundation of Korea through a grant provided by the Ministry of Science, ICT & Future Planning (NRF-2013R1A2A2A01067340), and by the National R&D Program through the Dong-nam Institute of Radiological & Medical Sciences (50491-2014).

References

1 A. Krása, V. Wagner, M. Majerle, F. Křížek, A. Kugler, O. Svoboda, J. Adam, M. Krivopustov, Nucl. Instrum. Methods A **615**, 70 (2010)
2 J. Vrzalová, O. Svoboda, A. Kugler, M. Suchopár, V. Wagner, Physics Procedia **31**, 126 (2012)
3 S. A. Kandil, B. Scholten, K. F. Hassan, H. A. Hanafi, S. M. Qaim, J. Radioanalytical. Nucl. Chem. **279**, 823 (2009)
4 A. V. Prokofiev, J. Blomgren, O. Byström, C. Ekström, S. Pomp, U. Tippawan, V. Ziemann, M. Österlund, Radiation Protection Dosimetry **126**, 18 (2007)
5 H. Schuhmacher, H. Brede, V. Dangendorf, M. Kuhfuss, J.-P. Meulders, W. Newhauser, R. Nolte, Nucl. Instrum. Methods A **421**, 284 (1999)
6 M. Baba, Y. Nauchi, T. Iwasaki, T. Kiyosumi, M. Yoshioka, S. Matsuyama, N. Hirakawa, T. Nakamura, S. Tanaka, S. Meigo, Nucl. Instrum. Methods A **428**, 454 (1999)
7 M. Österlund, J. Blomgren, S. Pomp, A. Prokofiev, U. Tippawan, L.-O. Andersson, T. Bergmark, O. Byström, H. Calén, L. Einarsson, Nucl. Instrum. Methods B **241**, 419 (2005)
8 P. Bém, V. Burjan, J. Dobes, U. Fischer, M. Götz, M. Honusek, V. Kroha, J. Novák, S. Simakov, E. Simecková, presented at the Proceedings of the International Conference on Nuclear Data for Science and Technology, 2007 (unpublished)
9 IAEA-EXFOR Database, at http://www-nds.iaea.org/exfor
10 A. J. Koning, D. Rochman, Nuclear data sheets **113**, 2841 (2012)
11 J. S. Hendricks, W. M. Gregg, L. F. Michael, R. J. Michael, C. J. Russell, W. D. Joe, P. F. Joshua, B. P. Denise, S. W. Laurie, W. M. William, LANL Report LA-UR-08-2216, Los Alamos (2008)
12 M. Zaman, G. Kim, H. Naik, K. Kim, S.-G. Shin, M. Tatari, M.-H. Cho, J. Radioanalytical. Nucl. Chem. **299**, 1739 (2014)
13 H. Naik, G. Kim, R. Schwengner, K. Kim, M. Zaman, M. Tatari, M. Sahid, S. Yang, R. John, R. Massarczyk, Nucl. Phys. A **916**, 168 (2013)
14 J. Blachot, C. Fiche, Ann. De Phys. **6**, 3 (1981)
15 R. Firestone, L. Ekström, WWW Table of Radioactive Isotopes, Ver. 2.1, URL http://ie.lbl.gov/toi/ (1999)